Thai Thanh Hiep
Lecturer
Department of Automotive Engineering, Faculty of Transportation Engineering
Ho Chi Minh City University of Technology (HCMUT), VNU-HCM, Ho Chi Minh City, Vietnam

Vu Viet Thang
Lecturer
Department of Automotive Engineering, Faculty of Transportation Engineering
Ho Chi Minh City University of Technology (HCMUT), VNU-HCM, Ho Chi Minh City, Vietnam

Hong Duc Thong
Doctor
Department of Automotive Engineering, Faculty of Transportation Engineering
Ho Chi Minh City University of Technology (HCMUT), VNU-HCM, Ho Chi Minh City, Vietnam

Dinh Quoc Tri
Lecturer
Department of Automotive Engineering, Faculty of Transportation Engineering
Ho Chi Minh City University of Technology (HCMUT), VNU-HCM, Ho Chi Minh City, Vietnam

Control of the Side Brush Street Sweeper for Various Road Surfaces Using PID and Sliding Mode Controllers

This paper examines the side brush control technologies for a novelty semi-autonomous road sweeper design. This study proposes a side brush structure and offers a brush control solution to improve working efficiency and reduce abrasive brush. For the mechanical system using a parallelogram mechanism, the direction of movement when raising and lowering the brush is always parallel to the road surface. The modeling of the side brush mechanism shows that this is a nonlinear system. Therefore, the Sliding Mode Control(SMC) was proposed and established from the dynamics equation. The Lyapunov theorem demonstrates its stability. Besides, we also consider the proportional-integral-derivative (PID) controller to evaluate the responsiveness of the linear controller for a nonlinear system. Finally, the parameters of the controllers are optimized by a genetic algorithm to consider the response of the sliding mode control compared to the PID controller to control the road sweeper side brush with different references.

Keywords: *Sliding Mode Control, Side brush, Street Sweeper, Road surfaces nonlinear system, PID controller, Genetic Algorithm (GA).*

1. INTRODUCTION

Nowadays, street sweepers are widely used to clean highways and industrial areas, etc. Most road sweepers use a device called a broom to sweep waste and use a unit to clean the dust suction or a conveyor to pick up the garbage. Usually, two rotating brooms are mounted on either side of the road sweeper to get rid of the debris near the side of the road. A long roller brush is placed at the rear of the vehicle or chassis to remove debris from the center of the road. A side brush sweeper consists of various crucial parts, which include load cell sensors to measure the force of the brush on the street, mechanical systems, a hydraulic cylinder, direction valves, etc.

The main components of the road sweeper, such as the side brush, main broom, cylinders, etc., must be included. The devices will be connected to a control panel in the cabin, and the driver must regularly observe the scan results to adjust accordingly, requiring the driver to have experience but also potentially dangerous when unable to concentrate on driving[1].

Previous studies have shown that side brush sweep about 80% of road debris in the region of the curb. Under the street sweeper, a roller brush removes the remaining 20% of the debris. Therefore, The design and automatic control of the road sweeper side brush are very important. It helps the street sweeper operate efficiently and reduces the complexity of the work for the driver [2], [3].

Received: January 2023, Accepted: May 2023
Correspondence to: Thai Thanh Hiep, Hong Duc Thong
Faculty of Transportation Engineering, Ho Chi Minh City University of Technology, Vietnam,
E-mail: thaithanhhiep@hcmut.edu.vn
doi: 10.5937/fme2303318H

In previous studies, the influence of road surface roughness on the brush system was not considered when designing the control system. Moreover, The mathe–matical model of these studies is a linear model with vertically mounted components that increase the height of the mechanism, which is difficult to install on an actual road sweeper. Some other studies use the linearization method of the side brush system, thus only considering the relatively small working area of the brush system.

We develop an automatic brush control system that is adapted to different road surface conditions through the control method of brush penetration or brush pressure. So as to control the sweeping force, the appropriate downward pressure can be used. As necessary for the sweeping conditions, the pressure should be changed. In order to achieve the above objectives, this study has proposed a mathematical model of the side brush based on the previous studies on the finite element model of the brush. Based on the mathematical model, the study uses the sliding mode controller and PID controller to examine the respon–siveness of the controllers to different road profiles. Road profiles are generated using the C class of road profiles defined by ISO 8608 standard, sinusoidal road profile, harversian road profile, and sine half-wave road profile [4],[5].

2. RELATED WORKS

In [2], research by Peel (2002) developed a design for a vehicle that sweeps roads semi-autonomously. How–ever, the waste identification and control system still needs to be created. Two brush types flicking brush and cutting brush have been given in his study. Besides,

theoretical steady-state modeling can determine the axial load, torque, and tine deflection geometry of these two brushes. In 2005, Wang [6] developed a Finite Element (FE) to study how debris interacts with brush tines through theoretical and experimental methods. The side brush parameters mentioned in his research as brushing force, tilt angle, and rotational speed. A pro–portional-derivative (PD) controller was used to improve the sweeping efficiency. Wang et al. [7] stu–died a mathematical regression model to summarize the FE model's results. The method could be used to predict features of different brushes under various operational variables. Useche et al. [8] evaluated the effectiveness of two-type tine brush, cutting and flicking (F128), under different operating conditions. Moreover, proper brush penetration, sweeper speed, and brush angle values for debris types were studied. Determine coeffi–cients of friction for cutting and F128 brushes studied by Useche et al. [9]. This study investigated the effects of the brush force in the cutting brush and the F128 brush. Useche et al. [10] presented an experimental method to determine suitable values of Rayleigh damping coefficients of tine brush and clusters brush. The effectiveness of the side brushes in removing different types of debris is studied by Useche et al. [11]. The experiment using a brushing test rig considered two different brush types, cutting and F128.Useche et al.[12]evaluated the dynamics of a novel free-rotating oscillating brush based on the authors' analytical model. Useche et al. [13] investigated the dynamics of the flic–king brush of a mathematical model when the brush was rotated freely. The dynamics and modeling of brushes are considered in research by Useche et al. [14], including the removal of fouling, post-CMP (Chemical Mechanical Polishing), street sweeping, etc. The FE model defines values of the normal contact stiffness, K_n, and Integration Time Step (ITS)[15]. In research [16], the dynamic FE model was developed to investigate how a cup-shaped brush's dynamics and performance are affected by brush oscillations. In research [17], The performance of two types of side brushes: a cutting brush and an F128 brush, was studied. Besides, their work developed the nonlinear FE brush model. In another study [18], a dynamic model of cutting brush was considered with the tine brush modeling as cantilever beams. The research by experimental tests [19] investigated the ability of the brush to remove the different debris kinds and various sweeping parameters. Wahab et al. [20] presented modeling a bristle of a brush for street sweeping by two FE models. In the first one, the bristle ends following a specific circular path under a specific time function. In the others, inertia loads are applied when the same bristle end is completely restricted. Peel et al. [21] developed a technical identification of different street surfaces and debris by vision processing. Yang et al. [22] conducted experimental research on the cleaning performance of the street sweeper. Moreover, the mathematical models were established with three main parameters driving speed, disc brush speed, and roller brush speed.

3. THE SIDE BRUSH SYSTEM OF THE STREET SWEEPER

3.1 The side brush road sweeper operation desc–ription

For most street sweepers, two rotary side brushes are mounted on both sides of a sweeper to remove the debris near the curb, as shown in Figure 1. At the same time, a roller brush is mounted beneath the chassis to clear the street center of debris.

This paper presented a design for the control system of the side brush mechanism. A hydraulic motor powers the rotating brush. In this research, the brushing force or brush penetration of the automatic side brush is controlled by a hydraulic cylinder and load cell.

a) Mechanical sweeper *b) The side brush*

Figure 1. The mechanical sweeper and the side brush [23]

The basic components of a side brush are given in Figure 2. The arm joints are parallelograms that help keep the brush direction parallel to the road surface.

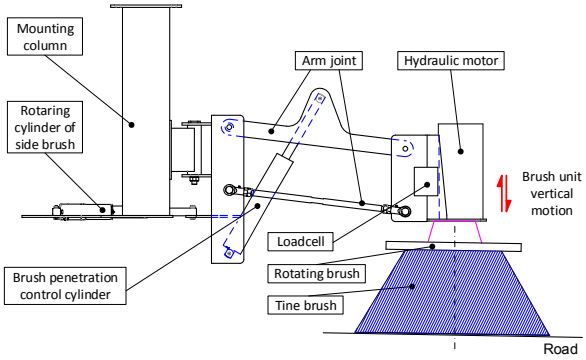

Figure 2. The basic components of the side brush

The measurement of the brush penetration is shown in Figure 3. The vertical height difference between a theoretically undeformed brush's lowest point and the road surface upon which the brush is deformed can be describe $\Delta = 0\,\mathrm{d}$ as the result when the brush is stationary and only touching the road surface.

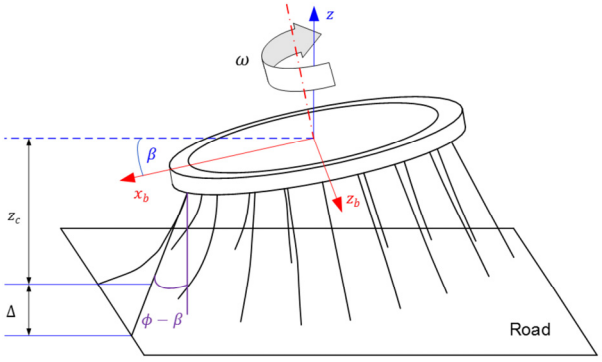

Figure 3. Definition of brush penetration [2]

It z_c is defined as the vertical distance between the road surface and the brush origin, then Figure 3 may be

used to construct an expression that connects the plane of the road to the point origin of the brush [2]:

$$z_c = R_{rj}.\sin\beta + L.\cos(\phi - \beta) - \Delta \quad (1)$$

where L is the length of the tine, R_{rj} is the largest mount radius, β is the assault angle for the brush, ϕ is the tine mount's angle, Δ and is the brush penetration.

3.2 The kinematics of side brush

The side brush is considered to be a simple mass-damping spring [6]. Since only the brush mechanism is evaluated at the operating position in Figure 2, it is not necessary to consider the side brush's mounting column and rotating cylinder. Therefore, the stitching and joint diagram of the side brush mechanism can be presented in Figure 4.

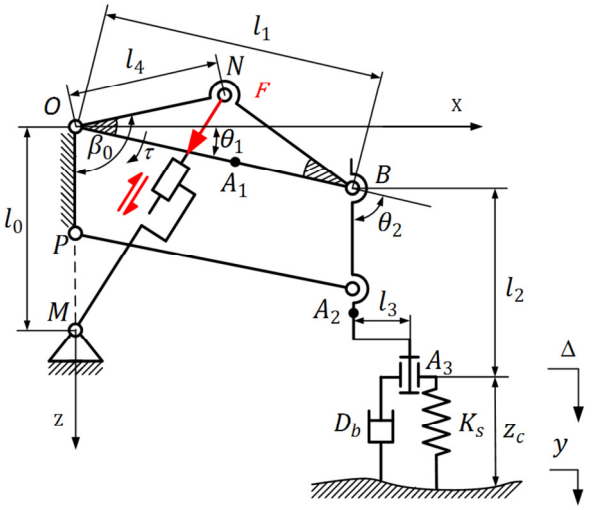

Figure 4. The side brush schematic

The kinematics schematic in Figure 4 shows that:

$$\theta_1 + \theta_2 = 90^0 \quad (2)$$

$$\dot{\theta}_1 + \dot{\theta}_2 = 0 \quad (3)$$

where θ_1 is the angle of link 1 (OB) from the Ox axis θ_2 is the angle of link 2 (BC) from link 1.

Link 1 (A_1) is the coordinates of the centers of mass (x_1,z_1) can be given as follows:

$$x_1 = \lambda_1 \cos\theta_1 \quad (4)$$

$$z_1 = \lambda_1 \sin\theta_1 \quad (5)$$

Link 2 (A_2) is the coordinates of the centers of mass (x_2,z_2) can be given as follows:

$$x_2 = l_1 \cos\theta_1 \quad (6)$$

$$z_2 = l_1 \sin\theta_1 + \lambda_2 \quad (7)$$

Link 3 (A_3) is the coordinates of the centers of mass (x_3,z_3) can be given as follows:

$$x_3 = l_1 \cos\theta_1 + l_3 \quad (8)$$

$$z_3 = l_1 \sin\theta_1 + l_2 \quad (9)$$

The symbols are given as follows: $|OA_1|=\lambda_1$, $|BA_2|=\lambda_2$,; JA_1, JA_2, JA_3 are the moments of inertia of links 1, 2, and 3 relative to their centers of mass, $\lambda_{1,2}$ are the coordinates of their mass centers, and y is the po–sition disturbances.

From considering the triangle area(OMN)can be the equation:

$$S_{OMN} = \frac{1}{2}OM.ON.\sin(\beta_0 + \theta_1) = \frac{1}{2}l_0.l_4.\sin(\beta_0 + \theta_1) \quad (10)$$

where β_0 is the initial angle of the angle MON.

The distance (MN) can be written by the formula:

$$MN = \sqrt{l_0^2 + l_4^2 - 2\cos\left((\beta_0 + \theta_1)\right)l_0 l_4} \quad (11)$$

3.3 The dynamic of the side brush

The system's kinetic and potential energies of link 1 can be written by the following equations:

$$K_1 = \frac{1}{2}m_1\left(\lambda_1\dot{\theta}_1\right)^2 + \frac{1}{2}J_{A1}\dot{\theta}_1^2 \quad (12)$$

$$P_1 = m_1 g\lambda_1 \sin\theta_1 \quad (13)$$

From equations (7), (8), the speed of the point A_2 can be determined as a function of the generalized coordinates θ_1, θ_2:

$$V_{A2}^2 = \dot{x}_2^2 + \dot{z}_2^2 = \left(\dot{\theta}_1 l_1 \sin\theta_1\right)^2 + \left(\dot{\theta}_1 l_1 \cos\theta_1\right)^2 = \dot{\theta}_1^2 l_1^2 \quad (14)$$

From equations (6), (7), the system's kinetic and potential energies of link 2 can be written:

$$K_2 = \frac{1}{2}m_2 V_{A2}^2 + \frac{1}{2}J_{A2}\dot{\theta}_2^{\,2} = \frac{1}{2}m_2\dot{\theta}_1^2 l_1^2 + \frac{1}{2}J_{A2}\dot{\theta}_1^2 \quad (15)$$

or

$$P_2 = m_2 g z_2 = m_2 g\left(l_1 \sin\theta_1 + \lambda_2\right) \quad (16)$$

It is easy to see that $VA_2 = VA_3$, $\theta_3 = 0$, from equations (8), (9), (12), the kinetic energy, the potential energy, and energy dissipation due to viscous friction of link 3 can be written:

$$K_3 = \frac{1}{2}m_3 l_1^2\dot{\theta}_1^2 \quad (17)$$

$$P_3 = m_3 g\left(l_1 \sin\theta_1 + l_2\right) + \frac{1}{2}K_s\left(l_1 \sin\theta_1 + l_3 \tan\theta_1 - y\right)^2 \quad (18)$$

$$R_3 = \frac{1}{2}D_b\left(l_1\dot{\theta}_1 \cos\theta_1 + l_3\dot{\theta}_1(\tan^2\theta_1 + 1) - \dot{y}\right)^2 \quad (19)$$

where K_s, D_b are the stiffness and damping coefficient, and y is the position disturbances of road profiles. They are representative of the brush's dynamic characteristics. In research [6], the FE modeling results indicate that K_s may vary from 1 kN/m to 50 kN/m when the side brush operates under different conditions.

Let's formulate the mechanism dynamics equation based on the second type of General Lagrange equation [24,25]:

$$\frac{d}{dt}\left(\frac{\partial K}{\partial \dot{q}_i}\right)-\frac{\partial K}{\partial q_i}+\frac{\partial R}{\partial \dot{q}_i}+\frac{\partial P}{\partial q_i}=Q_i \tag{20}$$

where K and P are the system's kinetic and potential energies, respectively; q is the generalized coordinate, Ris energy dissipation because of viscous friction Q_i is the corresponding loading in each coordinate.

The kinetic energy function:

$$K=\frac{1}{2}\left(m_1\lambda_1^2+m_2l_1^2+J_{A1}+J_{A2}\right)\dot{\theta}_1^2+\frac{1}{2}m_3l_1^2\dot{\theta}_1^2 \tag{21}$$

The first derivative of the kinetic energy function with respect to the variable $\dot{\theta}_1$:

$$\frac{\partial K}{\partial \dot{\theta}_1}=\left(m_1\lambda_1^2+J_{A1}+J_{A2}+m_2l_1^2+m_3l_1^2\right)\dot{\theta}_1 \tag{22}$$

The second derivative of the kinetic energy function with respect to the variable $\dot{\theta}_1$:

$$\frac{d}{dt}\frac{\partial K}{\partial \dot{\theta}_1}=\left(m_1\lambda_1^2+J_{A1}+J_{A2}+m_2l_1^2+m_3l_1^2\right)\ddot{\theta}_1 \tag{23}$$

The first derivative of the kinetic energy function with respect to the variable θ_1:

$$\frac{\partial K}{\partial \theta_1}=0 \tag{24}$$

The first derivative of the potential energy function with respect to the variable θ_1:

$$\begin{aligned}\frac{\partial P}{\partial \theta_1}&=\left(m_1g\lambda_1+m_2gl_1+m_3gl_1\right)\cos\theta_1+\\&K_s\left(l_1\sin\theta_1+l_3\tan\theta_1-y\right)\left[l_1\cos\theta_1+\right.\\&\left.l_3(\tan^2\theta_1+1)\right]\end{aligned} \tag{25}$$

The first derivative of the energy dissipation func–tion with respect to the variable $\dot{\theta}_1$:

$$\begin{aligned}\frac{\partial R}{\partial \dot{\theta}_1}&=D_b\left(l_1\dot{\theta}_1\cos\theta_1+l_3\dot{\theta}_1(\tan^2\theta_1+1)-\dot{y}\right)\\&\left(l_1\cos\theta_1+l_3(\tan^2\theta_1+1)\right)\end{aligned} \tag{26}$$

The total dynamics load can be written by the fol–lowing equations:

$$\begin{aligned}\tau&=\left(m_1\lambda_1^2+J_{A1}+J_{A2}+m_2l_1^2+m_3l_1^2\right)\ddot{\theta}_1+\\&D_b\left(l_1\dot{\theta}_1\cos\theta_1+l_3\dot{\theta}_1(\tan^2\theta_1+1)-\dot{y}\right)\\&\left(l_1\cos\theta_1+l_3(\tan^2\theta_1+1)\right)+K_s\left(l_1\sin\theta_1+l_3\tan\theta_1-y\right)\\&\left[l_1\cos\theta_1+l_3(\tan^2\theta_1+1)\right]\end{aligned} \tag{27}$$

From equations (10), (11), the moment generated by the hydraulic cylinder can be written by the following equations:

$$\tau=F\frac{2S_{OMN}}{MN}=F\frac{l_0.l_4.\sin(\beta_0+\theta_1)}{\sqrt{l_0^2+l_4^2-2\cos((\beta_0+\theta_1)l_0l_4}} \tag{28}$$

where F is the force generated by the hydraulic cylinder.

4. ROAD PROFILE

In order to simulate the side brush system that has been described, a sufficient model of the variation in the road surface, y(t), is required.

The sinusoidal road profile can be given using the following fundamental formulation [5,26]:

$$y(t)=H\sin\left(\frac{2\pi vt}{L}\right) \tag{29}$$

where v is the vehicle's speed, H is the bump height, L is the bump length $T = L/v$ and is the time to cross the bump.

Moreover, the bump can be modeled using the half-sine function [5][26]. The half-sine bump shape can be given by (29).

The half-sine model is somewhat harsh because, at time t = 0, its slope rapidly shifts from 0 to $2\pi H/T$ and thus, it needs a suitable model for a speed bump. Therefore the harversian function is a less severe bump model [5,26]:

$$y(t)=H\sin^2\left(\frac{\pi vt}{L}\right) \tag{30}$$

When performing more complex simulations, ran–dom variations that are based on statistical analyses of common road construction methods are sometimes used.

According to ISO 8608, the power spectral density (PSD) of profile elevations is given by the equation:

$$\Phi(\Omega)=\Phi(\Omega_0)\left(\frac{\Omega}{\Omega_0}\right)^{-w} \tag{31}$$

where $\Omega=2\pi/L$ in rad/m denotes the spatial angular velocity, $\Phi_0 = \Phi(\Omega_0)$ in rad/m is the PSD values at the reference spatial angular velocity Ω_0=1 rad/m, w is the amplitude reduction and w=2.

Besides, the road surface roughness (C class) in the time domain is as follows [4]:

$$y(t)=\sum_{n=1}^{N}B_n\sin(n\omega_0t-\psi_n) \tag{32}$$

where the amplitude B_n is defined as below:

$$B_n=\sqrt{\Phi(\Omega_i)\frac{\Delta\Omega}{\pi}},\ n=1,\ldots,N \tag{33}$$

in which $\Delta\Omega\equiv\frac{\Omega_N-\Omega_1}{N-1}$ (rad/ sec), and the phase ang–les ψ_n , n=1,……, N are considered to have a uniform distribution in the interval $[0,2\pi)$ and to be random variables.

Where the fundamental frequency of time:

$\omega_0\equiv V\Delta\Omega$, $\Delta\Omega\equiv 2\pi/L$, in which V is the vehicle velocity.

5. SLIDING MODE CONTROL, PID CONTROL, AND OPTIMIZING CONTROLLER PARAMETERS BY USING GENETIC ALGORITHM (GA)

5.1 Control System Analysis

A sliding mode controller that achieves robust control for uncertain systems combines the backstepping app–roach and sliding mode control. Let us assume the plant is a nonlinear system, as shown below [27]:

$$\begin{cases}\dot{x}_1 = x_2 \\ \dot{x}_2 = f(x,t) + b(x,t)u + d(x,t)\end{cases} \tag{34}$$

where $f(x,t)$, $b(x,t)$ and $d(x,t)$ are the nonlinear functions. Besides setting $x_1 = \theta_1$, $x_2 = \dot{\theta}_1$ obtains the following equations:

$$f(x,t) = -D_b x_2 \frac{\left(l_1 \cos x_1 + l_3(\tan^2 x_1 + 1)\right)^2}{\left(m_1\lambda_1^2 + J_{A1} + J_{A2} + m_2 l_1^2 + m_3 l_1^2\right)} - K_s \frac{\left(l_1 \sin x_1 + l_3 \tan x_1\right)\left[l_1 \cos x_1 + l_3(\tan^2 x_1 + 1)\right]}{\left(m_1\lambda_1^2 + J_{A1} + J_{A2} + m_2 l_1^2 + m_3 l_1^2\right)} \tag{35}$$

$$b(x,t) = \frac{1}{\left(m_1\lambda_1^2 + J_{A1} + J_{A2} + m_2 l_1^2 + m_3 l_1^2\right)} \frac{l_0 . l_4 . \sin(\beta_0 + x_1)}{\sqrt{l_0^2 + l_4^2 - 2\cos((\beta_0 + x_1) l_0 l_4}} \tag{36}$$

$$d(x,t) = \frac{D_b \dot{y}\left(l_1 \cos x_1 + l_3(\tan^2 x_1 + 1)\right)}{\left(m_1\lambda_1^2 + J_{A1} + J_{A2} + m_2 l_1^2 + m_3 l_1^2\right)} + \frac{K_s y\left[l_1 \cos x_1 + l_3(\tan^2 x_1 + 1)\right]}{\left(m_1\lambda_1^2 + J_{A1} + J_{A2} + m_2 l_1^2 + m_3 l_1^2\right)} \tag{37}$$

The following equation gives the output signal:

$$\begin{aligned}\Delta &= x_3 \tan\theta_1 \\ &= (l_1 \cos\theta_1 + l_3)\tan\theta_1 = l_1 \sin x_1 + l_3 \tan x_1\end{aligned} \tag{38}$$

5.2 PID control law design

The traditional PID controller's simplicity provides benefits for use in both linear and nonlinear systems. [28,29] The PID controller's mathematical formulation is as follows:

$$u(t) = K_p e(t) + K_i \int e(t) + K_d \frac{d}{dt} e(t) \tag{39}$$

Tracking error:

$$e = y - \Delta \tag{40}$$

where u(t) is the input signal and the error signal e(t). The PID controller's goal is still to reduce error by gra–dually fine-tuning the control variable u(t). The resul–ting error value, however, is calculated continuously, and the PID controller makes adjustments based on the proportional gain (k_p), integral gain (k_i), and derivative gain (k_d).

However, because k_p, k_i, and k_d are frequently fixed, the PID controller struggles to deal with system uncertainties, including parameter fluctuations and outside disturbances. Therefore, a more reliable cont–roller design has been necessary in recent years in order to enhance system performance by removing parametric uncertainties and outside disturbances.

5.3 Sliding mode control law design

The dynamics of a nonlinear system are changed via sliding mode control. This nonlinear control technique uses numerous control structures to ensure that trajec–tories always move in the direction of a switching con–dition [27,30].

Select Lyapunov function:

$$V = \frac{1}{2}\sigma^2 \tag{41}$$

The derivative Lyapunov function:

$$\dot{V} = \sigma\dot{\sigma} \tag{42}$$

Select the sliding mode function:

$$\sigma = \dot{e} + c_1 e \tag{43}$$

For $\sigma \to 0$, it is necessary to select the control signal u(t) so that $\dot{V} < 0$:

$$\begin{aligned}\dot{\sigma} &= \ddot{e} + c_1\dot{e} \\ &= \ddot{y} - \ddot{\Delta} + c_1\dot{e} \\ &= -\left(l_1 \cos x_1 + l_3 \tan^2 x_1\right)\left(f(x,t) + b(x,t)u + d(t)\right) \\ &+ \ddot{y} + c_1\dot{e} + l_1\dot{x}_1^2 \sin x_1 - l_1\dot{x}_1^2 \tan x_1(\tan^2 x_1 + 1)\end{aligned} \tag{44}$$

The control signal u(t) using saturation function:

$$u(t) = \frac{1}{b(x,t)\left(l_1 \cos x_1 + l_3 \tan^2 x_1\right)}\Big[\ddot{y} + c_1\dot{e} + l_1\dot{x}_1^2 \sin x_1 - l_1\dot{x}_1^2 \tan x_1(\tan^2 x_1 + 1) + Ksat(\sigma)\Big] - \frac{f(x,t) + d(t)}{b(x,t)} \tag{45}$$

From the above control law, there is the equation:

$$\dot{V} = -K\sigma sat(\sigma) < 0 \;\; \forall\sigma \neq 0, \;\; K > 0 \tag{46}$$

where K represents a constant rate.

Saturation function:

$$sat(\sigma) = \begin{cases} 1, & \sigma > \gamma \\ \dfrac{\sigma}{\gamma}, & |\sigma| \le \gamma \\ -1, & \sigma < \gamma \end{cases} \tag{47}$$

where γ is the boundary layer.

The control signal u(t) using relay function:

$$u(t) = \frac{1}{b(x,t)\left(l_1 \cos x_1 + l_3 \tan^2 x_1\right)}\Big[\ddot{y} + c_1\dot{e} + l_1\dot{x}_1^2 \sin x_1 - l_1\dot{x}_1^2 \tan x_1(\tan^2 x_1 + 1) + Krelay(\sigma)\Big] - \frac{f(x,t) + d(t)}{b(x,t)} \tag{48}$$

Relay function:

$$\eta(\sigma) = \frac{s}{|s| + \delta} \tag{49}$$

where δ is a very small positive constant.

5.4 Controller parameters optimization by GA

The original goal of the GA, which was to create autonomous learning and decision-making systems, was to simulate the biological processes of natural selection and population genetics. GA is often used to create high-quality solutions to global optimization and find issues by utilizing operators inspired by biology, such as mutation, crossover, and selection [31].

The four fitness functions commonly used to evalu–ate trajectory trackings such as Integral Absolute Error (IAE), Integral Square Error (ISE), Integral Time Abso–lute Error (ITAE), and Integral Time Square Error (ITSE). These are defined by the following equation [32,33]:

$$J_{IAE} = \int_0^{+\infty} |e(t)| dt \tag{50}$$

$$J_{ISE} = \int_0^{+\infty} e^2(t) dt \tag{51}$$

$$J_{ITAE} = \int_0^{+\infty} t|e(t)| dt \tag{52}$$

$$J_{ITSE} = \int_0^{+\infty} te^2(t) dt \tag{53}$$

ISE integrates the square of the error over time; control systems designed to minimize ISE have a tendency to eradicate major errors swiftly but will tolerate minor bugs that last for a long time.

IAE integrates the absolute error over time, though typically with less persistent oscillation, it tends to yield slower responses than ISE optimum systems.

ITAE integrates the absolute error multiplied by the time over time. It considers weight errors that exist at the beginning of the response far more significantly over time [34][35].

Thoroughly reflect the operating state of the system and consider accumulated errors. Therefore, this paper selected the ITSE as the consideration function [36]. ITSE integrates time the square error over time, allowing for a faster control speed than ITAE. It is the only objective function for optimization by GA.

Table 1. Operators of GA techniques used to determine the best PID and SMC gains.

Option	Value/ type	
	PID	SMC
No of variables	3	2
Population size	20	20
Crossover	0.9	0.9
Mutation	0.1	0.1
Fitness function	ITSE	ITSE

One of the research about PID parameters optimi–zation using GA was studied by Aly [37]. Besides, sliding mode control based on GA was also studied by Kheshti et al. [38] and Ma et al [39]. Table 1 shows the evaluated values of GA parameters so that the GA tunes the PID and SMC gains.

6. RESULTS AND DISCUSSIONS

The side brush model of the street sweeper is designed by Solid Works software (Figure 5). The parts of the model are the mounting column, rotating cylinder of the side brush, arm joint, hydraulic motor, and rotating brush. The rotating cylinder of the side brush is controlled ON/OFF. When the road sweep system operates, it takes the side brush in the working position and brings the side brush inward in the vehicle moving on the road. Research results focus only on controlling brush penetration through PID and sliding mode control. GA optimizes the parameters of the controller.

The side brush's kinematic measurements are as below: $l_0 = 0.322\,\text{m}$, $l_1 = 0.45\,\text{m}$, $l_2 = 0.254\,\text{m}$, $l_3 = 0.145\,\text{m}$, $l_4 = 0.242\,\text{m}$, $\lambda_1 = 0.23\,\text{m}$, $\lambda_2 = 0.105\,\text{m}$.

$m_1 = 8.2\,\text{kg}$, $m_2 = 9.7\,\text{kg}$, $m_3 = 40\,\text{kg}$, $J_{A1} = 0.18\,\text{kg.m}^2$, $J_{A2} = 0.05\,\text{kg.m}^2$.

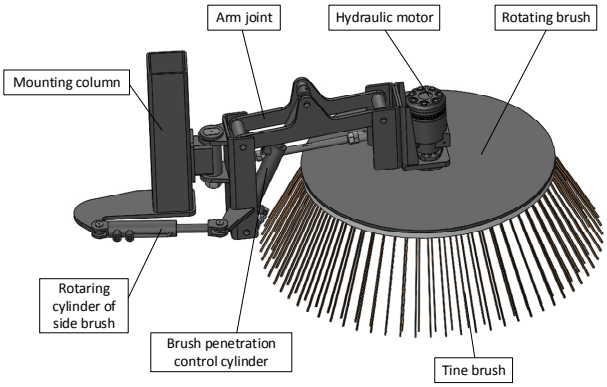

Figure 5. The side brush model

The parameters for PID [k_p, k_i, k_d] in Table 1 and the parameters for SMC [K, c_1] in Table 2 were tuned by the ITSE fitness function. Moreover, the various road profiles were considered to evaluate the responsiveness of the controller. The GA-SMC uses functions such as a sign, sat, and relay to consider the nonlinear controller. The parameters were tuned and presented in Table 2.

Table 2. PID tuned by the ITSE fitness function

GA-PID	Road profile			
	Sinusoidal	Half-sine	Haversine	C class
K_p	13288000.4	12641972.9	11168000.7	5729100
K_i	609.928	597.518	99.384	2.61
K_d	47703.55	66899.88	41899.95	43607
J	$2.2519.10^{-4}$	0.0015	$1.8299.10^{-4}$	0.7056

Table 3. SMC tuned by the ITSE fitness function

GA-SMC		Road profile			
		Sinusoidal	Half-sine	Haversine	C Class
Using *sign* function	K	93870.18	91768.1	84870.9	65786
	c_1	90.311	33.95655	419.694	91.811
	J	$1,776.10^{-15}$	$2,106.10^{-14}$	$3,771.10^{-14}$	$1,709.10^{-6}$

Using *sat* function	K	92369.57	128473,14	38994.74	79001.37
	c_1	94.734	82,794	46.646	13.281
	J	$1{,}764.10^{-13}$	$3{,}99.10^{-14}$	$2{,}221.10^{-16}$	$7{,}511.10^{-9}$
Using *relay* function	K	867,27	985,82	946.18	3943.7
	c_1	660,07	571,87	683.72	2.2535
	J	$2{,}223.10^{-16}$	$2{,}230.10^{-16}$	$2{,}65.10^{-16}$	$1{,}501.10^{-6}$

The penetration of the side brush (see Figure 6) is forced to track the nominal road profiles. The genetic artificial-based proportional-integral-derivative (GAPID) and the genetic artificial-based sliding mode control (GASMC) are designed to consider the responsiveness of linear (PID) and nonlinear (SMC) controllers. Besides, the GASMC uses sign function (GASMC-sign) in practical engineering systems; the chattering of SMC can cause damage to system parts such as the actuator. One way to reduce the chattering is to use the saturation function (GASMC-sat) and relay function (GASMC-relay) instead of the sign function.

It can be seen that the real and reference trajectory curves both almost match after about 0,1s in road profiles: sinusoidal, half-sine, and harversian. The random profile also tracks quite well on trajectory curves. Figure 6 and Figure 7 shows the response and tracking error levels of control laws and road profiles. The GAPID has a short settling time, but it fluctuates widely in the initial period. The GASMC-sat and GASMC-relay show a good response and reduced chattering.

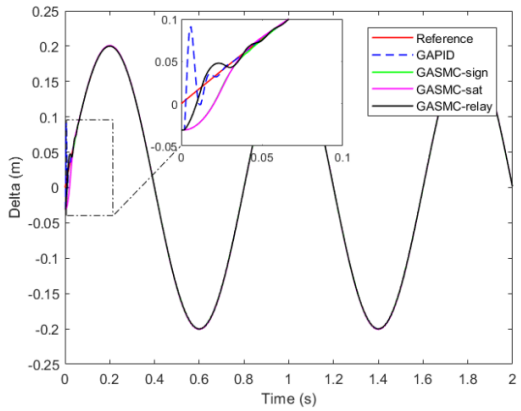

a) Sinusoidal

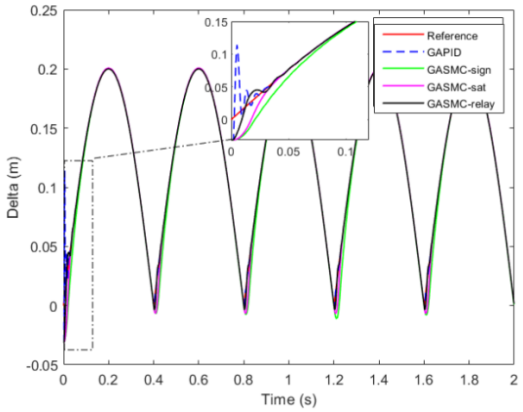

b) Half-sine

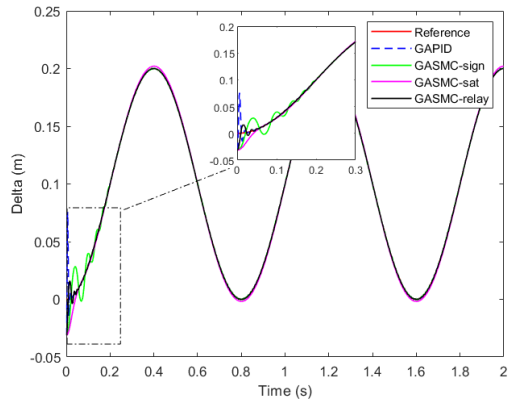

c) Haversine

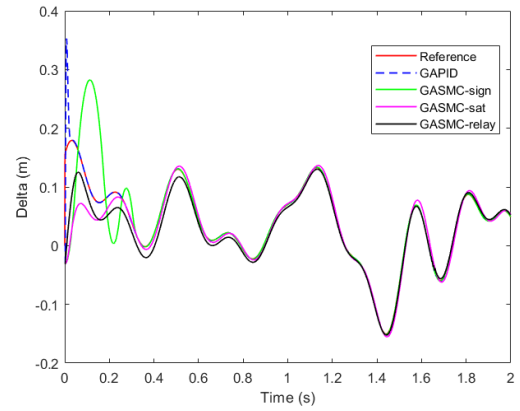

d) Random (C class)

Figure 6. The tracking position of the side brush

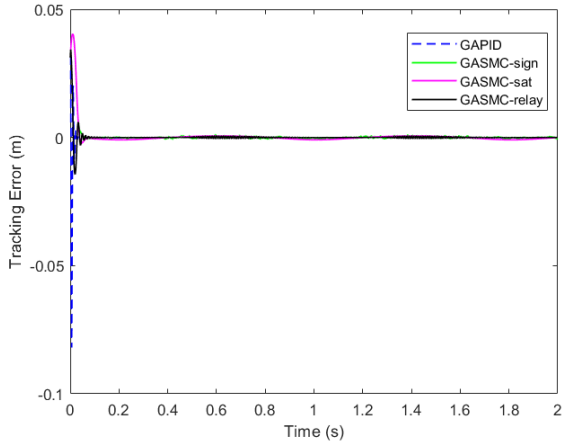

a) Sinusoidal

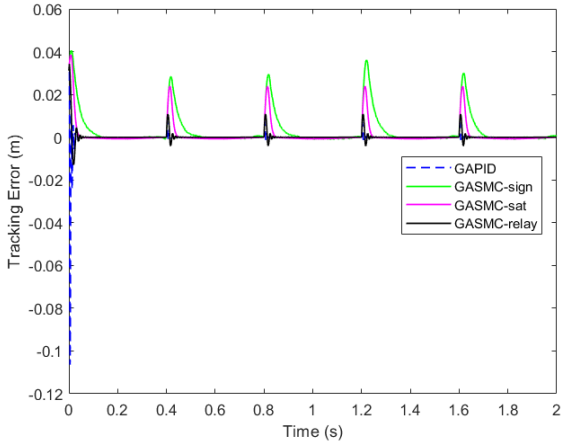

b) Half-sine

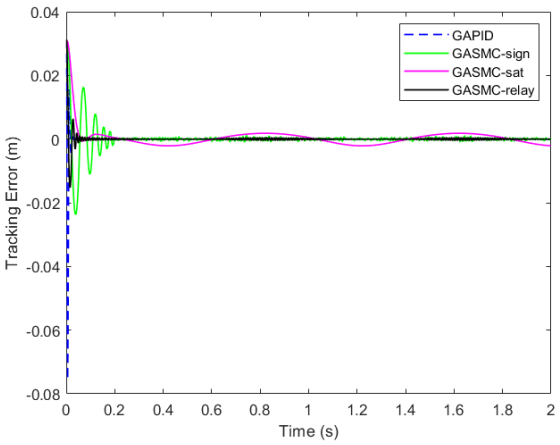

c) Haversian

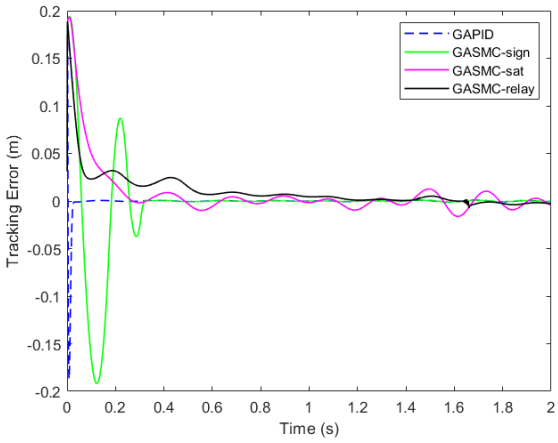

d) Random (C class)

Figure 7. The tracking error of the side brush position

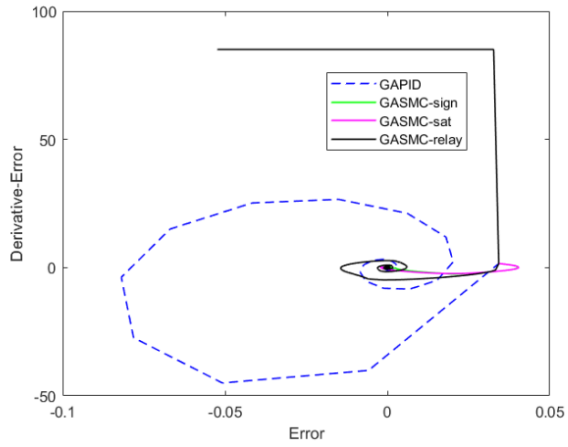

a) Sinusoidal

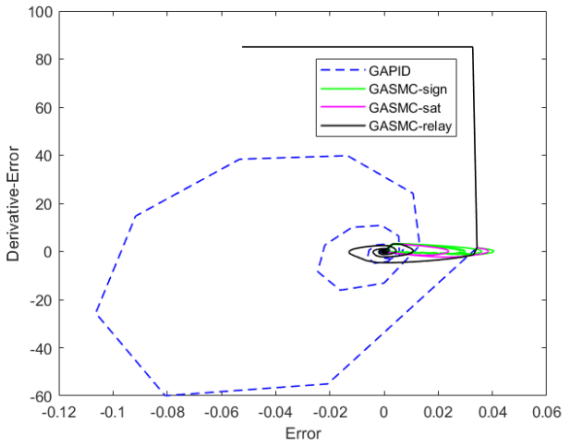

b) Half-sine

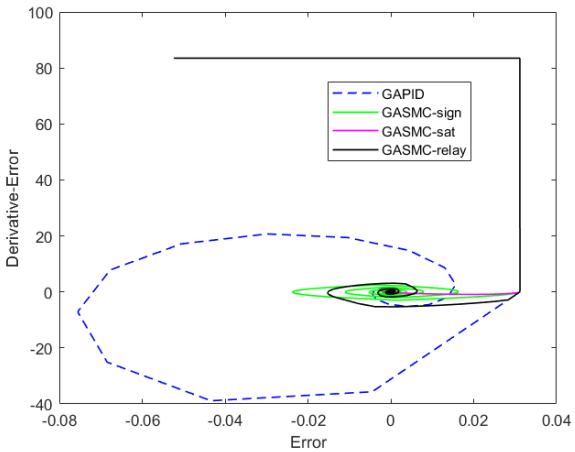

c) Haversian

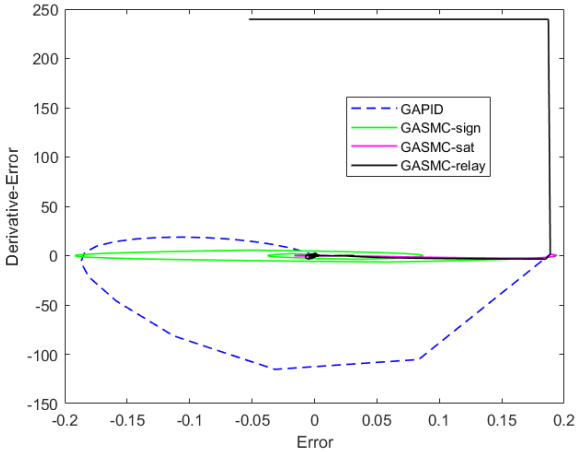

d) Random (C class)

Figure 8. The phase trajectory of the side brush position

The error of position tracking and phase trajectory for the side brush is presented in Figure 7 and Figure 8. The tracking error of the side brush position after settling time (t_s =0,4s) is less than 0.025 m. Finally, Figure 8 shows the phase trajectory of the side position of control rules for different road profiles.

7. CONCLUSION

This paper suggests a technique to automatically control the road sweeper's side brush to improve working efficiency and reduce brush wear. The paper uses different control laws and various road profiles to consider the level of response. GA optimizes the parameters of the controller.

Simulations have been performed for four different types of road surfaces, and the results show that the side brush system controllers are designed to track different types of road surfaces. The simulation results show that the GAPID controller fluctuates with large amplitude (tracking error 0,075-0,187m) in a very short period of time (0.005-0.008s) at the initial time, which can cause damage to the mechanical systems of the side brushes.

The GASMC-sat and the GASMC-relay have a pretty good response in road profiles and reach a steady state after about 0.3s. With the road profiles such as sinu–soidal, half-sine, and harversian, the controllers respond quite well. However, the random road profile is only the GASMC-sat and the GASMC-relay having a relatively good response. Besides, this study is given a novel method to control the side brush of the road sweeper. This method can be easily applied on road sweepers due to the automatic control of the brush by the hydraulic cylinder.

ACKNOWLEDGMENT

We acknowledge Ho Chi Minh City University of Technology (HCMUT), VNU-HCM, for supporting this study.

REFERENCES

[1] Wang, C., Parker, G.: Analysis of Rotary Brush Control Characteristics for a Road Sweeping Robot Vehicle, in: International Conference on Mechatronics and Control (ICMC), 03-05 July 2014, Jinzhou (China), pp. 1799-1804.

[2] Peel, G.: A General Theory for Channel Brush Design for Street sweeping, PhD thesis, School of Engineering, University of Surrey, Surrey, 2002.

[3] Wahab, M.A, Parker, G., Wang, C.: Modelling rotary sweeping brushes and analyzing brush characteristic using finite element method, Finite Elements in Analysis and Design, Vol. 43, No. 6-7, pp. 521–532, 2007.

[4] Tyan, F., Hong, Y.F., Tu, S.H., Jeng, W.S.: Generation of Random Road Profiles, Journal of Advanced Engineering, Vol. 4, No. 2, pp. 151–156, 2009.

[5] Goodarzi, A., Khajepour, A.: Vehicle Suspension System Technology and Design, Morgan & Claypool, Waterloo, 2017.

[6] Wang, C.: Brush Modelling and Control Techniques for Automatic Debris Removal during Road Sweeping, PhD thesis, School of Engineering, University of Surrey, Surrey, 2005.

[7] Wang, C., Sun, Q., Wahab, M.A., Zhang, X., Xu, L.: Regression modeling and prediction of road sweeping brush load characteristics from finite element analysis and experimental results, Waste Management, Vol. 43, pp. 19–27, 2015.

[8] Useche, L.V.V., Wahab, M.M.A., Parker, G.A.: Effectiveness of oscillatory gutter brushes in removing street sweeping waste, Waste Management, Vol. 43, pp. 28–36, 2015.

[9] Useche, L.V.V., Wahab, M.M.A., Parker, G.A.: Determination of friction coefficients, brush contact arcs and brush penetrations for gutter brush road interaction through FEM, Acta Mechanica, Vol. 221, No. 1-2, pp. 119–132, 2011.

[10] Useche, L.V.V., Wahab, M.M.A., Parker, G.A.: Determination of the Rayleigh damping coefficients of steel bristles and clusters of bristles of gutter brushes, Dyna, Vol. 82, No. 194, pp. 230–237, 2015.

[11] Useche, L.V.V., Wahab, M.M.A., Parker, G.A.: Effectiveness of gutter brushes in removing street sweeping waste, Waste Management, Vol. 30, No. 2, pp. 174-184, 2010.

[12] Useche, L.V.V., Wahab, M.M.A., Parker, G.A.: Dynamics of a freely rotating cutting brush subjected to variable speed, International Journal of Mechanical Sciences, Vol. 50, No. 4, pp. 804-816, 2008.

[13] Useche, L.V.V., Wahab, M.M.A., Parker, G.A.: Dynamics of an unconstrained oscillatory flicking brush for road sweeping, Journal of Sound and Vibration, Vol. 307, No. 3-5, pp. 778-801, 2007.

[14] Useche, L.V.V., Wahab, M.M.A., Parker, G.A.: Brush dynamics: models and characteristics, in: Proceedings of ESDA2006 8th Biennial ASME Conference on Engineering Systems Design and Analysis, 04-07 July 2006, Torino (Italia), pp. 1-10.

[15] Useche, L.V.V., Wahab, M.M.A., Parker, G.A.: Determination of the normal contact stiffness and integration time step for the finite element modeling of bristle-surface interaction, Computers, Materials & Continua, Vol. 56, No. 1, pp. 169-184, 2018.

[16] Useche, L.V.V., Wahab, M.M.A., Parker, G.A.: Dynamic finite element model of oscillatory brushes, Finite Elements in Analysis and Design, Vol. 47, pp. 771-783, 2011.

[17] Useche, L.V.V., Wahab, M.M.A., Parker, G.A.: Numerical Analysis of Tilted Cutting and F128 Brushes, Computer Modeling in Engineering & Sciences, Vol. 121, No. 1, pp. 23-47, 2019.

[18] Useche, L.V.V., Wahab, M.M.A., Parker, G.A.: Modeling of an oscillatory freely-rotating cutting brush for street sweeping, Dyna, Vol. 78, No. 170, pp. 204-213, 2011.

[19] Wahab, M.M.A., Wang, C., Useche, L.V.V., Parker, G.A.: Experimental determination of optimum gutter brush parameters and road sweeping criteria for different types of waste, Waste Management, Vol. 31, No. 6, pp. 1109-1120, 2011.

[20] Wahab, M.M.A., Useche, L.V.V., Parker, G.A.: Comparison of two finite element models of bristles of gutter brushes for street sweeping, International Journal of Fracture Fatigue and Wear, Vol. 3, pp. 221-226, 2015.

[21] Peel, G., Michielen, M., Parker, G.: Some aspects of road sweeping vehicle automation, in: Proceedings of the 2001 IEEE/ASME International Conference in Advanced Intelligent Mechatronics, 08-12 July 2001, Como (Italia), pp. 337-342.

[22] Yang, Q., Zhou, Y., Ying, K., Li, R, Wang, X.: Study on Cleaning Performance of Small Road Sweeper Vehicle, in:3rd International Conference on Electrical, Automation and Mechanical Engineering, 24-25June 2018, Xi'an (China), pp. 194-198.

[23] DucLong Auto, https://www.duclongauto.com/xe-chuyen-dung/xe-quet-duong-conveyor-5000-255.html.

[24] Huertasa, V.V., Ilkiva, B.R.: Vibration Suppression of a Flexible Structure, in: Procedia Engineering, Vol. 48, pp. 233-241, 2012.

[25] Amouri, A., Cherfia, A., Merabti, H., Leksir, Y.L.D.: Nonlinear Model Predictive Control of a Class of Continuum Robots Using Kinematic and Dynamic Models, FME Transactions, Vol. 50, No. 2, pp 339–350, 2022.

[26] Palm III, W. J.:System Dynamics, McGraw-Hill Education, New York, 2021.

[27] Liu, J., Wang, X.: Advanced Sliding Mode Control for Mechanical Systems, Tsinghua University Press, Beijing and Springer-Verlag Berlin Heidelberg, 2012.

[28] Noordin, A., Basri1, M.A.M, Mohamed, Z., Lazim, I.M.: Adaptive PID Controller Using Sliding Mode Control Approaches for Quadrotor UAV Attitude and Position Stabilization, Arabian Journal for Science and Engineering, 2020.

[29] Belkhiri, A., Amouri, A., Cherfia, A.: Design of Fractional-Order PID Controller for Trajectory Tracking Control of Continuum Robots, FME Transactions, Vol. 51, No. 2, pp. 243–252, 2023.

[30] Cömert, C., Kasnakoğlu, C.: Comparing and Developing PID and Sliding Mode Controllers for Quadrotor, International Journal of Mechanical Engineering and Robotics Research, Vol. 6, No. 3, pp. 194-199, 2017.

[31] Ahmmed, T., Akhter, I., Karim, S.M.R., Ahamed, FAS: Genetic Algorithm Based PID Parameter Optimization, American Journal of Intelligent Systems, Vol. 10, No. 1, pp. 8-13, 2020.

[32] Kumar, I., Kushwaha, K.: Optimization of Automatic Voltage Regulator Using Genetic Algorithm Applying IAE, ITAE Criteria, International Journal of Engineering Research and Applications, Vol. 6, No. 3, pp. 20-24, 2016.

[33] Mok, R., Ahmad, M.A.: Fast and optimal tuning of fractional order PID controller for AVR system based on memorizable-smoothed functional algorithm, Engineering Science and Technology, an International Journal, Vol. 35, pp. 1-15, 2022.

[34] Measures of controlled system performance https://www.online-courses.vissim.us/Strathclyde/measures_of_controlled_system_pe.htm.

[35] Jovanovic, R., Bugaric, U.S., Vesovic, M.V., Perisic, N. B.: Fuzzy Controller Optimized by the African Vultures Algorithm for Trajectory Tracking of a Two–Link Gripping Mechanism, FME Transactions, Vol. 50, No. 3, pp. 491–501, 2022.

[36] Fan, Y., Shao, J., Sun, G., & Shao, X.: Proportional–Integral–Derivative Controller Design Using an Advanced Lévy-Flight Salp Swarm Algorithm for Hydraulic Systems, Energies, Vol. 13, No. 2, pp. 1-20, 2020.

[37] Aly, A.A.: PID Parameters Optimization Using Genetic Algorithm Technique for Electrohydraulic Servo Control System, Intelligent Control and Automation, Vol. 2, pp. 69-76, 2011.

[38] Kheshti, M.R. et al.: Genetic Algorithm-Based Sli–ding Mode Control of a Human Arm Model, IFAC-Papers On-Line, Vol. 55, No. 10, pp. 2968-2973, 2022.

[39] Ma, Y. M., & Dou, F. J.: Application of Sliding Mode Control Based on Genetic Algorithm in direction Control System of Submarine, in : 2012 International Conference on Computer Science and Service System, 11-13 August 2012, Nanjing (China), pp. 1518-1521.

NOMENCLATURE

Δ	The brush penetration
L	The length of the tine
R_{rj}	The largest mount radius
B	The assault angle for the brush
ϕ	The tine mount's angle
θ_1	The angle of link 1 from the Ox
θ_2	The angle of link 2 from link 1
$\lambda_{1,2}$	The coordinates of mass centers
y	The position disturbances
J_A	The moments of inertia of links relative to their centers of mass.
β_0	The initial angle of the angle $\widehat{MON}$
V_A	The speed of the center of mass
Ks	The stiffness of the side brush
D_b	Damping coefficient
K	The system's kinetic energy
P	The system's potential energy
q	The generalized coordinate
R	The energy dissipation
Q_i	The corresponding loading in each coordinate
τ	The total dynamics load
F	The force generated by the hydraulic cylinder
H	The bump height
L	the bump length
T	The time to cross the bump
Ω	The spatial angular velocity
Φ	The power spectral density
w	The amplitude reduction
B_n	The amplitude of the road surface roughness (C class)
ψ_n	The phase angles
V	The vehicle velocity
γ	The boundary layer
δ	The very small positive constant

Abbreviations

SMC	Sliding Mode Control
GA	Genetic Algorithm
FE	Finite Element
PD	Proportional-Derivative
PID	Proportional-Integral-Derivative
F128	Flicking brush (The bristle mount orientation angle is 128 degrees)

CMP	Chemical Mechanical Polishing
ITS	Integration Time Step
PSD	Power Spectral Density
IAE	Integral Absolute Error
ISE	Integral Square Error
ITAE	Integral Time Absolute Error
ITSE	Integral Time Square Error

КОНТРОЛА МАШИНЕ ЗА ЧИШЋЕЊЕ УЛИЦА СА БОЧНОМ ЧЕТКОМ ЗА РАЗЛИЧИТЕ ПОВРШИНЕ ПУТЕВА КОРИСТЕЋИ ПИД И КОНТРОЛЕРЕ КЛИЗНОГ РЕЖИМА

Т.Т. Хиеп, В.В. Танг, Х.Д. Тонг, Д.К. Три

Овај рад испитује тehнологије управљања бочним четкицама за нови дизајн полуаутономне машине за чишћење путева. Ова студија предлаже структуру бочне четке и нуди решење за контролу четкица за побољшање радне ефикасности и смањење абразивне четке. За мehанички систем који користи мehанизам паралелограма, смер кретања при подизању и спуштању четке је увек паралелан са површином пута.

Моделирање мehанизма бочне четке показује да се ради о нелинеарном систему. Због тога је предложена и успостављена контрола клизног режима (СМЦ) из једначине динамике. Теорема Љапунова показује њену стабилност. Осим тога, разматрамо и пропорционално-интегрално-деривативни (ПИД) регулатор за процену одзива линеарног регулатора за нелинеарни систем. Коначно, параметри контролера су оптимизовани генетским алгоритмом како би се размотрио одзив контроле клизног режима у поређењу са ПИД контролером за контролу бочне четке машине за чишћење пута са различитим референцама.